Improvements to Lunar BRDF-Corrected Nighttime Satellite Imagery: Uses and Applications

Tony A. Cole[1], Andrew L. Molthan[2], Lori A. Schultz[3], Miguel O. Roman[4], David W. Wanik[5]

[1]Oak Ridge Associated Universities, ORNL, [2]NASA Marshall Space Flight Center, [3]Earth System Science Center, UA Huntsville, [4]NASA Goddard Space Flight Center, [5]Department of Civil & Environmental Engineering, University of Connecticut

Observations made by the VIIRS day/night band (DNB) provide daily, nighttime measurements to monitor Earth surface processes. However, these observations are impacted by variations in reflected solar radiation on the moon's surface. As the moon transitions from new to full phase, increasing radiance is reflected to the Earth's surface and contributes additional reflected moonlight from clouds and land surface, in addition to emissions from other light sources observed by the DNB. The introduction of a bi-directional reflectance distribution function (BRDF) algorithm serves to remove these lunar variations and normalize observed radiances. Provided by the Terrestrial Information Systems Laboratory at Goddard Space Flight Center, a 1 km gridded lunar BRDF-corrected DNB product and VIIRS cloud mask can be used for a multitude of nighttime applications without influence from the moon. Such applications include the detection of power outages following severe weather events using pre- and post-event DNB imagery, as well as the identification of boat features to curtail illegal fishing practices. This presentation will provide context on the importance of the lunar BRDF correction algorithm and explore the aforementioned uses of this improved DNB product for applied science applications.

Lunar BRDF-Corrected VIIRS DNB Imagery

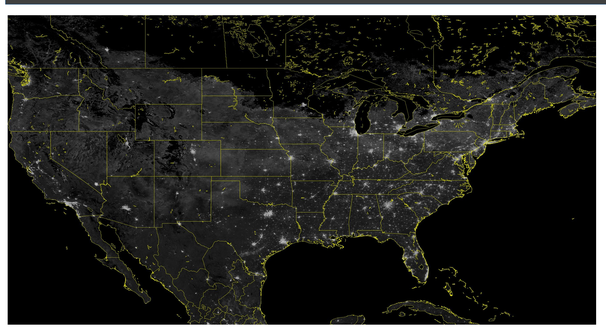

Figure 1: Version 1.0 lunar BRDF-corrected DNB composite using a **seasonally-estimated** BRDF correction. Image displays mean pixel radiances from nightly observations during 2013. Ability to see land surface indicates limited effectiveness of the BRDF algorithm in its current form.

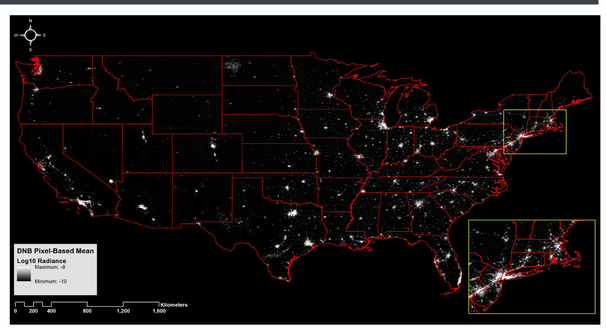

Figure 2: Version 5.0 lunar BRDF-corrected DNB composite using a **nightly-calculated** BRDF correction. Image displays mean pixel radiances from nightly observations between 2012 and 2015. Inability to see land surface indicates improved effectiveness of the BRDF algorithm.

Estimating Power Outages Using Pre- and Post-event Imagery

- **90-night pre-event minimum composite image**
  - Provide "normal" city light baseline
- **Single-night, post-event image(s)** immediately following the event and into the recovery phase
- Percent of Normal calculation:
  - Pre-event composite is differenced from each available post-event single image to determine **percent of normal emissions** using:

$$Percent_{normal} = 100 * \left(\frac{Post}{Pre}\right)$$

- Resulting product assigns a percent of normal value (0% to 100%) to each available, cloud-free pixel

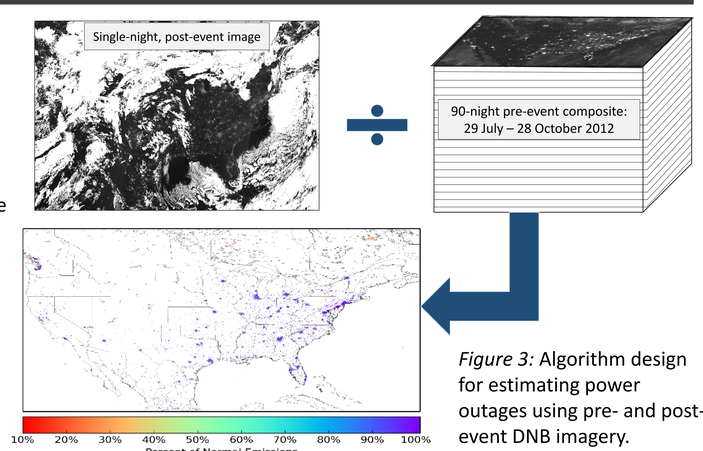

Figure 3: Algorithm design for estimating power outages using pre- and post-event DNB imagery.

Estimating Power Outages: Hurricane Sandy

Figure 4: Visual and numerical impact of Hurricane Sandy on the eastern U.S. seaboard.

VIIRS Outage Detection

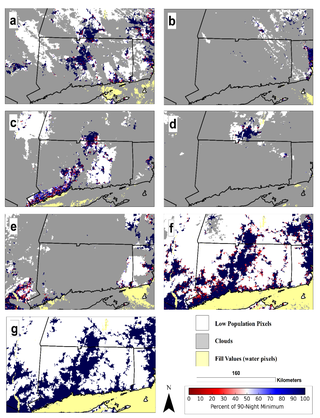

Figure 5: Nightly percent of normal products following Hurricane Sandy. Panels correspond to post-event products on a) 30 October, b) 31 October, c) 1 November, d) 2 November, e) 3 November, f) 4 November, and g) 6 November 2012, respectively.

UConn Validation Dataset

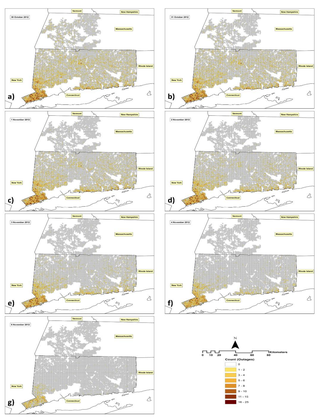

Figure 6: Locations of known power outages following Hurricane Sandy. Panels correspond to post-event products on a) 30 October, b) 31 October, c) 1 November, d) 2 November, e) 3 November, f) 4 November, and g) 6 November 2012, respectively.

Predication Model Error Statistics

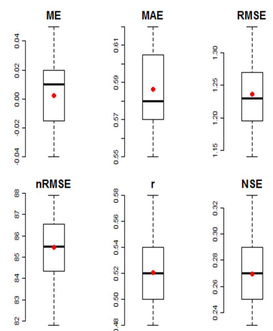

Figure 7: Error metrics from neural network outage prediction model, with a 20-fold cross-validation, following Hurricane Sandy. Metrics include mean error (ME), mean absolute error (MAE), root mean square error (RMSE) and Nash-Sutcliffe efficiency (NSE). Metrics were calculated from 1-km grid cells for each fold (n=20 folds).

Detecting Illegal Fishing Vessels: South China Sea

OUR OCEAN WASHINGTON, DC 2016

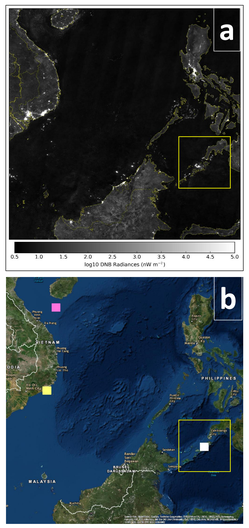

Figure 8: South China Sea test domain.
a) Composite of the DNB radiance data
b) Map of domain with algorithm development domains shown. Domain 3 shown in yellow

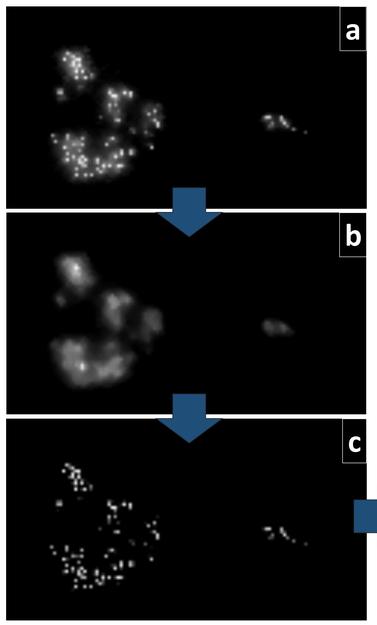

Figure 9: Algorithm design for detecting fishing vessels in the South China Sea.
a) Unfiltered, lunar BRDF-corrected DNB image,
b) Median filtered DNB image and
c) Spike Median Index (SMI) image for 7 October 2015.

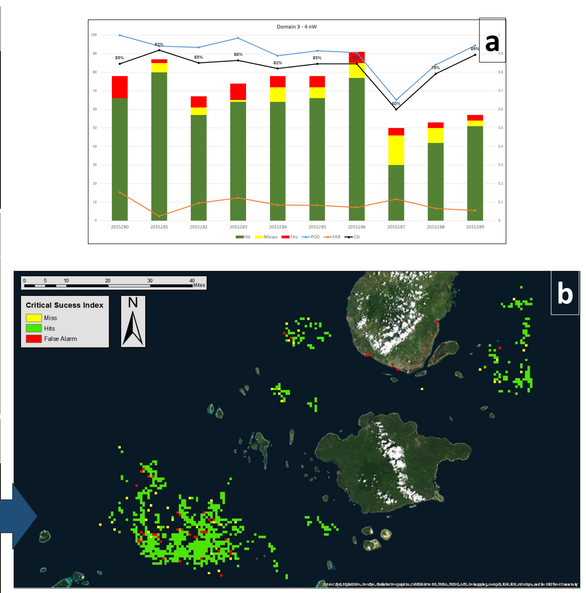

Figure 10: Comparison to an independent validation dataset was accomplished for each of the three subdomains over a ten-day period.
a) Critical Success Indices (CSI, Schaefer, 1990) were calculated. A bar plot of the Hits, Misses, False Alarms (FAs) are shown with line plots of the Probability of detection (POD), False Alarm Rate (FAR) and CSI.
b) Corresponding map of the Domain 3 hits, misses and FAs.